Analyst

PAPER

View Article Online
View Journal | View Issue

CrossMark click for updates

Cite this: *Analyst*, 2016, **141**, 5627

A "chemical nose" biosensor for detecting proteins in complex mixtures†

Jacob L. Rogowski,[a,b] Mohit S. Verma,[a,b] Paul Z. Chen[a,b] and Frank X. Gu*[a,b]

A growing understanding of the fundamental role of proteins in diseases has advanced the development of quantitative protein assays in the medical field. Current techniques for protein analysis include enzyme-linked immunosorbent assays (ELISA), flow cytometry, mass spectrometry, and immunohistochemistry. However, many of these conventional strategies require specialized training, expensive antibodies, or sophisticated equipment, raising assay costs and limiting their application to laboratory analysis. Here, we present the application of a "chemical nose" type colorimetric gold nanoparticle sensor for detection, quantification, and identification of single proteins, protein mixtures, and proteins within the complex environment of human serum. The unique interactions between a mixture of two different gold nanoparticle morphologies (spherical and branched) and six separate proteins (bovine serum albumin, human serum albumin, immunoglobulin G, fibrinogen, lysozyme, and hemoglobin) generated distinguishable protein- and concentration-dependent absorption spectra, even at nanomolar concentrations. Furthermore, we show that this response is sensitive to the relative abundance of different proteins in solution, permitting analysis of protein mixtures. Finally, we demonstrate the ability to distinguish human serum samples with and without a clinically relevant two-fold increase in immunoglobulin G, without the use of expensive reagents or complicated sample processing.

Received 28th March 2016,
Accepted 15th July 2016

DOI: 10.1039/c6an00729e

www.rsc.org/analyst

Published on 15 July 2016. Downloaded by Harvard University on 14/10/2016 16:45:31.

Introduction

Protein detection, identification, and quantification assays have diverse applications ranging from biomedical diagnostics and health monitoring,[1–3] to environmental[4,5] and consumer protection.[6,7] While several methods for protein identification are commercially available, many conventional methods such as ELISA are not well-suited for consumer level or point-of-care applications due to procedural complexity, equipment requirements, or high assay cost. Furthermore, these assays generally rely on "lock and key" models for protein detection, whereby a specific antibody is required to detect a protein of interest and detection of multiple proteins requires several antibodies. The detection of multiple analytes simultaneously, commonly referred to as multiplexing, allows for more complete analysis of biological samples. However, multiplexed protein analysis often employs several probes (*e.g.* protein microarray)[8] or specialized equipment such as mass spectrometers.[2]

Increasing accessibility of multiplexed protein analysis will require the development of new biosensing techniques that lower the cost and equipment requirements. Colorimetric nanosensor platforms are increasingly studied for biosensing applications in research, clinical, and consumer level environments due to their ease-of-use, and high sensitivity.[9–11] Among these platforms, gold nanoparticles are popular due to their unique optical properties.[12,13] As the particle size increases, or particles aggregate in solution, their electromagnetic absorption peak shifts to longer wavelengths.[14–16] Since the peak wavelengths for gold nanoparticles typically fall within the visible range of the electromagnetic spectrum, these shifts can be perceived as changes in color without specialized equipment.

One common method for protein detection using gold nanoparticles is to functionalize them with target-specific probes such as antibodies, peptides, or aptamers. These surface-bound molecules can then bind to freely diffusing proteins, thereby forming inter-particle bridges and producing a colorimetric response. However, this "lock and key" strategy for detecting proteins suffers from similar limitations to conventional methods. As a result, probe-functionalized gold nanoparticles are not optimal for low-cost broad-spectrum protein analysis. Another strategy relies on the displacement of a fluorophore from the gold nanoparticle by a target analyte.[17] In this case, the analyte presence is monitored by changes in fluorescence rather than absorbance. An array of nanoparticles

[a]*Department of Chemical Engineering, University of Waterloo, 200 University Avenue W, Waterloo, Ontario, N2L 3G1, Canada. E-mail: frank.gu@uwaterloo.ca; Fax: +1 519-888-4347; Tel: +1 519-888-4567 x 38605*
[b]*Waterloo Institute for Nanotechnology, University of Waterloo, 200 University Avenue W, Waterloo, Ontario, N2L 3G1, Canada*
†Electronic supplementary information (ESI) available. See DOI: 10.1039/c6an00729e

Published on 15 July 2016. Downloaded by Harvard University on 14/10/2016 16:45:31.

with different surface modifications and protein interactions can be used to establish an identifying fingerprint, but the need for fluorophores and fluorescence measurements raises manufacturing and equipment requirements.

While certain strategies use probes for protein-specific binding, it is also well known that protein adsorption can occur non-specifically on the surface of both metallic and non-metallic nanoparticles.[18–20] The collection of proteins adsorbed onto the surface of these nanoparticles is known as the protein corona and has been shown to affect the stability of nanoparticle solutions. For instance, many studies suggest that adhesion of proteins onto gold nanoparticles can increase their stability and may prevent *in vivo* aggregation.[21,22] Other studies show that the presence of certain proteins can destabilize nanoparticle solutions.[19,23,24] Furthermore, the degree of protein coverage and particle stability is often related to the protein concentration.[19,25] While the effect of protein adsorption and corona formation on nanoparticle stability is commonly studied due to its impact on diagnostic and therapeutic platforms, a few studies have investigated how these non-specific interactions can be used for protein identification and sensing.[23,26–28]

In a "chemical nose" system, several different responses to a single analyte are used to construct a unique fingerprint for that analyte, thereby improving distinction over a single-response system.[29–33] This approach has been previously demonstrated for detection of bacteria using gold nanoparticles.[31] Since the nanoparticle morphology plays a key role in protein–nanoparticle aggregation, the response of different shapes can also be used in a "chemical nose" for improved distinction between proteins. In this study, we show that branched and spherical cetyltrimethylammonium bromide-(CTAB)-coated gold nanoparticles (Fig. S1†) produce unique colorimetric responses to different proteins, and that a 1 : 1 (v : v) mixture of the two (from now on, referred to as "chemical nose" solution) can be used to discriminate between six proteins: bovine serum albumin (BSA), human serum albumin (HSA), immunoglobulin G (IgG), lysozyme (Lyz), fibrinogen (Fib), and hemoglobin (Hgb). We also demonstrate how the relative abundance of proteins in a binary mixture can be determined based on this response. Finally, we use this platform to detect elevated globulin levels in human serum, which can serve as an indicator of the disease status and a predictor of mortality in cancer patients.[34–39]

Results and discussion

Ionic strength

The majority of protein detection and identification experiments are performed in aqueous solutions. Since it has been shown that ions can mediate both the colloidal stability of gold nanoparticles in solution,[40,41] as well as the electrostatic interaction between proteins and gold nanoparticles,[42] it was important to choose a salt concentration which would maximize the performance of our assay. In the absence of proteins, high salt concentrations can be used to destabilize gold nanoparticles.[43,44] With proteins in solution, the ionic composition of a medium can affect both protein–protein interactions[45] and protein adsorption on surfaces.[46] To determine the optimal ionic concentration for protein-induced "chemical nose" aggregation, serial dilutions of BSA were prepared in deionized water, saline (NaCl), or phosphate-buffered saline (PBS) at varying salt concentrations, such that the final ionic strengths of NaCl and PBS were 450, 112.5, or 28.125 μM (from now on referred to as 1×, 1/4×, and 1/16×, respectively). These concentrations were chosen since they are below the experimentally observed salt concentration which causes gold nanoparticle aggregation.

In all the observed cases, protein solutions dissolved in PBS induced nanoparticle aggregation at lower protein concentrations than those dissolved in NaCl with the same ionic strength (Fig. S2†). This suggests that polyionic species (*e.g.* phosphate groups in PBS) have a larger effect on mediating nanoparticle aggregation. The increase in aggregation at lower protein concentrations is favourable for high sensitivity detection assays. Additionally, the solutions of 1/4× NaCl and 1/4× PBS outperformed their higher and lower ionic strength counterparts, while pure deionized Millipore H_2O was the least sensitive (Fig. S2†). These findings suggest the existence of an optimal ionic environment which facilitates protein-induced nanoparticle aggregation. For optimal performance at low concentrations, subsequent experiments were performed by diluting the protein and/or serum in 1/4× PBS.

Shape-dependent response

In order to have good distinction between proteins, it is necessary to obtain several unique responses to the same analyte. The proteins can then be identified based on their unique fingerprint or pattern of responses. One simple method for changing the response of gold nanoparticles is to change their morphology. By changing the gold nanoparticle shape (*i.e.* from spherical to branched) we can alter their optical absorbance spectra and how they interact with their environment. This technique has been previously demonstrated only for the detection of bacteria.[29–31,47,48]

Here, we have optimized the detection conditions to obtain a differential response in the presence of different proteins. To determine whether these two nanoparticle morphologies respond differently to proteins, we incubated the spherical, branched, and a 1 : 1 mixture of both with BSA, IgG, and a protein-free medium (1/4× PBS). At a concentration of 150 nM, both BSA and IgG induced nanoparticle aggregation, as evidenced by decreases in absorbance intensity, red-shifting of the spectrum, and broadening of the absorption peak (Fig. 1).

A difference in responses between spherical and branched morphologies was also apparent. While the absorbance peak for branched nanoparticles was completely flattened in the presence of both BSA and IgG, BSA only induced partial flattening in spherical nanoparticles (Fig. 1B) whereas IgG induced complete flattening (Fig. 1C). For both proteins and the negative control, the absorbance of the "chemical nose"

 This journal is © The Royal Society of Chemistry 2016

Published on 15 July 2016. Downloaded by Harvard University on 14/10/2016 16:45:31.

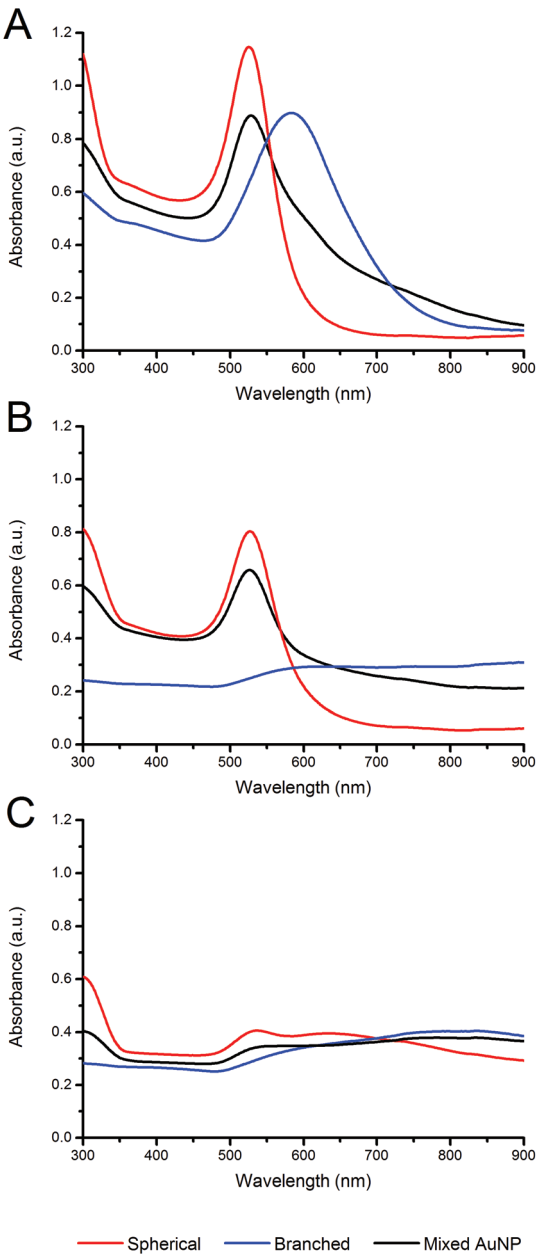

Fig. 1 Absorbance spectra for spherical, branched, and mixed (spherical and branched, 1 : 1 by volume) nanoparticle solutions when incubated with (A) PBS, (B) 150 nM BSA, or (C) 150 nM IgG. Average curves are shown (n = 8).

solution is a hybrid of both spherical and branched curves, suggesting that both nanoparticle morphologies maintain their individual behaviours when mixed together. The combination of two or more nanoparticle morphologies in this manner can provide added discriminatory power from a single sample well, thereby simplifying the assay.[30]

Concentration-dependent response

Several investigations have observed concentration-dependent effects of proteins on gold nanoparticle aggregation and adsorption.[23,28] Despite extensive interest in the field, many confounding factors make characterization of the aggregation mechanisms difficult. Observed effects can be influenced by the protein identity,[49] protein concentration,[23] nanoparticle coatings (*e.g.* PEGylated surfaces,[24] citrate-stabilization or CTAB-stabilization[21,50]), medium (*e.g.* DI H_2O, PBS,[50] NaCl,[22] citrate[21]), and experimental set-up.[19,23] To determine the concentration-dependent aggregation of CTAB-coated gold nanoparticles to the proteins in this study, fifteen 2× serial dilutions were prepared for each protein in 1/4× PBS. The resulting protein concentrations ranged from 450 μM to 27.46 nM (BSA, HSA, Lyz, Hgb) and from 28.125 μM to 1.72 nM (IgG, Fib). The lower concentrations of IgG and Fib were used due to preliminary results, which showed higher sensitivity to these proteins. By combining these solutions (100 μL) with gold nanoparticles (200 μL) in a 96-well plate, the final protein concentrations were further diluted to one third of these values. A negative control containing only 1/4× PBS serves as a baseline for comparison. Within 1 minute of nanoparticle addition, several protein dilutions displayed a visible change in color when compared to the negative control. This color change progressed rapidly for the first 10 minutes of incubation. To allow sufficient time for the assay color to stabilize, samples were incubated for 20 hours under dark ambient conditions. Fig. 2 shows the resulting aggregation response curves, presented as a peak-height difference between the sample and control.

Each protein exhibits a unique concentration-dependent aggregation curve. Furthermore, while BSA and HSA share similar structures, isoelectric points, and 76% amino acid sequence identity, their response curves are clearly distinguishable. While some proteins (BSA, HSA, IgG) lead to significant changes in absorbance over a wide range of concentrations (73 μM to 5 nM), others respond only at certain concentrations (Fib, Hgb), and the remainder produce little

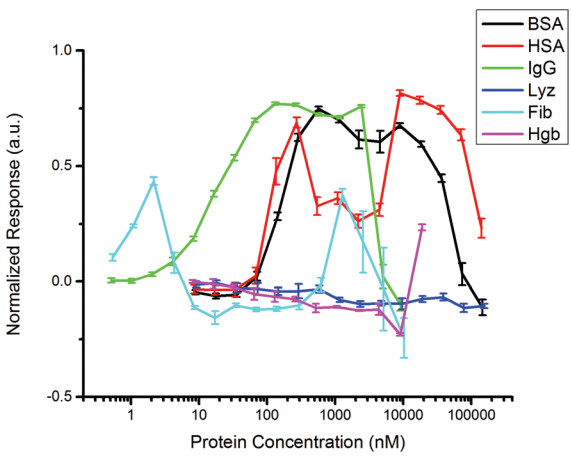

Fig. 2 Concentration-dependent aggregation of the CTAB-stabilized "chemical nose" to different proteins. Higher normalized response, defined as the difference in absorbance peak height between sample and control, indicates more aggregation. Mean response values (n = 3) are presented as ±S.D.

Published on 15 July 2016. Downloaded by Harvard University on 14/10/2016 16:45:31.

or no response (Lyz). The bell-shaped response common to BSA, HSA, and IgG suggests the existence of different aggregation regimes for high, moderate, and low protein concentrations. Previous studies have described similar bell-shaped response curves when exposing negatively-charged polystyrene and PMMA nanoparticles to IgG.[19,51] Cukalevski *et al.* proposed that high protein concentrations saturate the particle surface, reducing the overall aggregate size, while intermediate concentrations allow for aggregation by bridge formation where a single protein can bind to more than one nanoparticle.[19] A different study showed that progressive addition of BSA to a citrate-stabilized gold-nanoparticle solution led to an increase in aggregation up to a saturation point beyond which no more aggregation occurred.[23] It is likely that the bell-shaped response was not observed by this group since the protein concentration was steadily increased and irreversible particle aggregation occurred before the surface was saturated with protein. In our parallel comparison of several different proteins under identical conditions, we were able to discern varying ranges of aggregation and sensitivity.

The lower limits of detection were calculated based on linear regression analysis of the linear response range. The results of this analysis are presented in ESI Table S1† alongside the physiological concentrations of proteins in clinical samples. The detection limits range from 0.3 nM to 127 nM for proteins which had linear ranges within the concentration range studied (BSA, HSA, IgG, Fib). Neither hemoglobin nor lysozyme caused significant aggregation at the concentrations studied. Only the highest concentration of hemoglobin produced measurable aggregation. As such, these samples had insufficient information to calculate a lower limit of detection.

The irregular bell-shaped response curve makes data interpretation more difficult than for assays with regular sigmoidal response curves. While the low concentration linear range for proteins studied was relatively narrow (*e.g.* 71–284 nM for BSA, 1–16 nM for IgG, 0.5–2 nM for Fib), the upper limit of detection can be expanded and a wide range of concentrations can still be determined through sample dilution. For instance, an undiluted sample of BSA which produces a small but measurable degree of aggregation could be diluted 10× and 100×. If these dilutions result in a decrease in aggregation, the undiluted sample would be on the low end of the concentration–response curve. If these dilutions result in an increase in aggregation, the undiluted sample would be on the high end of the concentration–response curve. These responses could then be compared to a calibration curve to quantify the protein concentration. Optimum strategies for quantification that yield the highest accuracy are currently under investigation.

Protein identification

The ability to distinguish between different proteins is another valuable aspect of broad-spectrum biomolecular sensing. A multiplexed system of functionalized gold nanoparticles where different nanoparticles bind to different targets has been proposed, but the requirement to have one nanoparticle per protein limits the variety of proteins which can be identified.[52] To assess the potential for protein discrimination at nanomolar concentrations using non-specific gold nanoparticle solutions, we prepared six protein solutions and normalized their concentration to 450 nM using absorbance at 280 nm. Each protein was then incubated with the "chemical nose" solution such that the final protein concentration was 150 nM. Within 1 minute of gold nanoparticle addition, BSA, HSA, and IgG were noticeably different in appearance than the 1/4× PBS control. The differences between Fib, Lyz, Hgb, and control were less noticeable. Even after 20 hours of incubation, these samples were not appreciably different to the unaided eye. Following incubation, full spectral scans revealed protein-dependent variations in the absorption spectra. Average absorption curves for each protein are plotted in Fig. 3A showing the difference between equimolar solutions. The contour plot in Fig. 3B highlights the sample-to-sample similarity of the 6 proteins, where the horizontal layers within each plot represent 8 replicates. PCA classification of these spectra established that

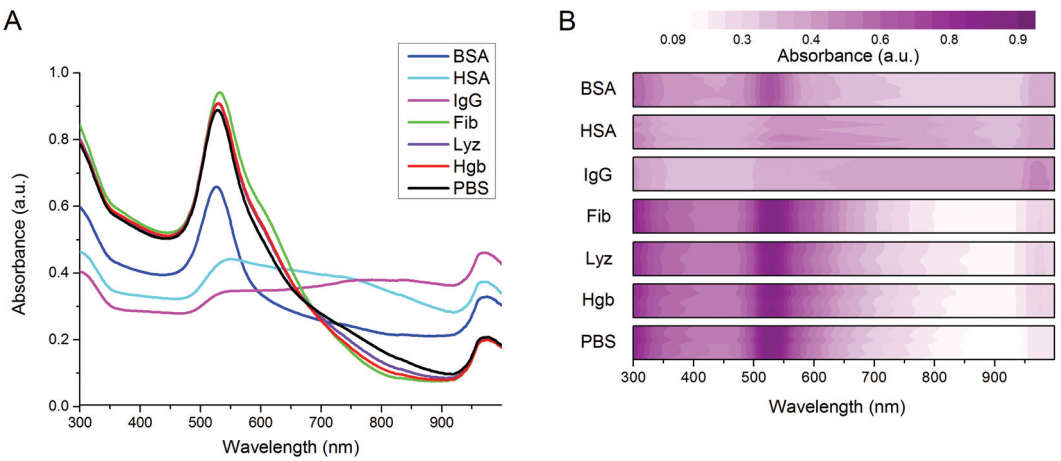

Fig. 3 Absorption spectra for "chemical nose" solutions with 6 different protein samples at 150 nM. (A) Average absorption curves (n = 7 or 8) highlight differences between proteins. (B) Contour plots of individual absorption curves (n = 7 or 8) highlighting the similarity between replicates.

This journal is © The Royal Society of Chemistry 2016

Published on 15 July 2016. Downloaded by Harvard University on 14/10/2016 16:45:31.

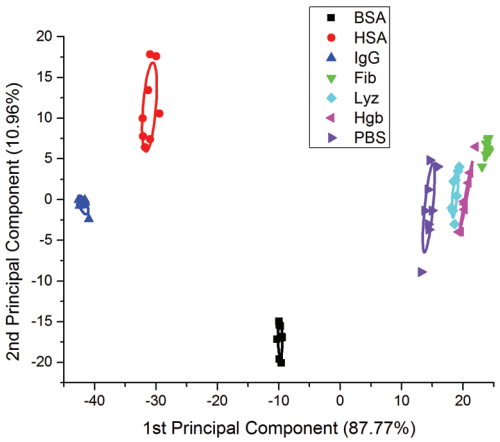

Fig. 4 Principal Component Analysis (PCA) biplot of the "chemical nose" response to different proteins at 150 nM. Ellipses represent 95% mean confidence levels.

the first two principal components could account for 98.7% of the observed variability. A biplot of PCA scores in Fig. 4 shows the grouping of samples based on their protein identity. While large separation was observed for those proteins producing a visually noticeable response (BSA, HSA, and IgG), even those solutions which were not appreciably different to the naked eye (*i.e.* Fib, Lyz, Hgb) could be resolved using PCA classification (Fig. 4). In order to assess cluster separation, cross-validation was performed by randomly selecting three samples of each protein to serve as the training set in the initial PCA, followed by linear discriminant analysis of the remaining 34 unknown samples (4–5 per protein) based on the PCA coefficients from the training set. This method resulted in a classification accuracy of 100%. Unlike the biplot in Fig. 4, classification was performed using the first three principal components. Inclusion of the third principal component aids in discriminating amongst those proteins with smaller separation on a two principal-component plot (*i.e.* Lyz, Hgb, and Fib).

The mechanism of protein-induced aggregation is a popular topic for recent studies investigating protein–gold nanoparticle interactions. Many factors have been identified which may influence these interactions, including the nanoparticle and protein charges,[26,53–55] polymeric coatings,[18,42,56] ionic strength,[42,57] nanoparticle morphology,[49,58,59] protein conformation,[23] and amino acid composition.[60,61] Of these parameters, electrostatic interactions between proteins and gold surfaces are most commonly used to explain protein adsorption and corona formation. This may explain why cationic CTAB-coated gold nanoparticles experience little or no aggregation upon exposure to Lyz. Since the high isoelectric point of Lyz (pI = 11) renders it positively charged under experimental conditions, we may expect electrostatic repulsion between proteins and nanoparticle surfaces. However, adsorption has been reported between like-charged proteins and nanoparticles,[50] which suggests that opposite charges are not necessary for protein adsorption. While a precise mechanistic understanding of each protein is not required in order to observe differences in stability and associate these responses with given samples, ongoing studies aim to identify which parameters contribute most strongly to differential nanoparticle–protein interactions as this will help direct assay development and optimization.

Protein mixtures

While the detection and quantification of single proteins is often useful in research environments, many samples may contain mixtures of proteins. In particular, clinical samples used for diagnostics will almost certainly contain a variety of different proteins and components. The "chemical nose" solution was combined with binary mixtures of HSA and IgG to determine whether their relative abundance affects the observed response. For each mixture, the total protein concentration was held constant at 150 nM and the mole fraction of HSA was set to 75%, 50%, or 25%. These samples were also compared to the single protein solutions containing 150 nM HSA and 150 nM IgG. As is shown in the resulting PCA biplot (Fig. 5), samples containing only HSA or 150 nM IgG form two separate clusters, while the mixtures fall in between the two. This suggests that the absorption spectra for the binary mixtures of HSA and IgG contain features of both pure solutions. It is interesting to note that while the clusters for mixed samples fall between HSA and IgG, they are not evenly spaced as may be expected if both proteins contribute equally to the response. In fact, 25% and 50% HSA lie closer to IgG than HSA, and 75% HSA falls near the midpoint between the two populations. This is likely due to the fact that 150 nM IgG has a stronger aggregating effect compared to 150 nM HSA (Fig. 2 and 3), and therefore the cluster position is weighted not only by the protein mole fraction but also by the aggregating strength. As previously described for the protein identification results (Fig. 4), cross-validation was performed by randomly selecting 3 samples from each protein to serve as a training set for PCA, followed by classification of the remaining 24

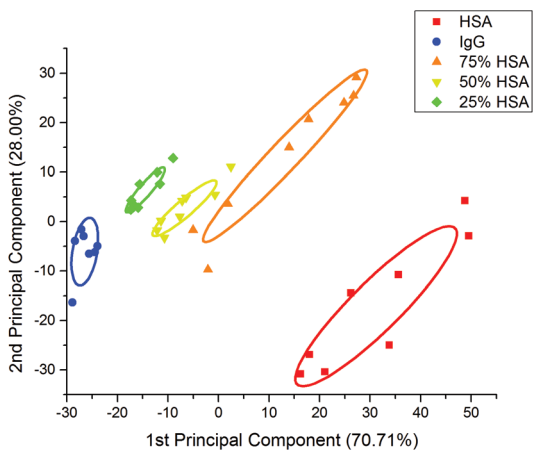

Fig. 5 Principal Component Analysis (PCA) plot of "chemical nose" response to different mixtures of proteins. Composition reflects the mole fraction of HSA in the 150 nM total protein (HSA + IgG) concentration. Ellipses represent 95% mean confidence levels.

Published on 15 July 2016. Downloaded by Harvard University on 14/10/2016 16:45:31.

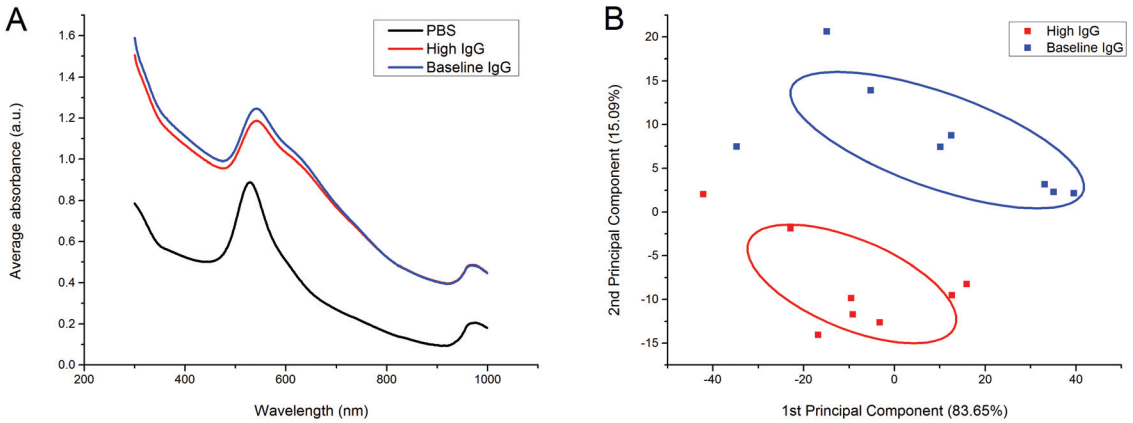

Fig. 6 (A) Mean absorption spectra for "chemical nose" solutions with serum containing baseline and high IgG (n = 8). (B) Principal Component Analysis (PCA) plot of the "chemical nose" response to serum containing high and baseline IgG. Ellipses represent 95% mean confidence levels. The observed decrease in the peak height between baseline and high IgG was statistically significant at $p < 0.01$.

samples per protein using linear discriminant analysis. Using the first three principal components, 22/24 samples were correctly classified (91.7%). The two misclassifications occurred between the adjacent concentration groups, which suggests that although we may not be able to determine very fine concentration values and identify proteins simultaneously, coarse protein concentrations and protein identities can still be distinguished in mixtures.

Complex media

The quantification of protein levels in complex media such as serum can be used to diagnose a multitude of diseases.[2,34,35] Total protein and the albumin/globulin ratio (AGR) are among the routine tests ordered by health care providers in determining a patient's health status. In particular, low pretreatment AGR is often associated with increased mortality in cancer patients and may be a valuable predictor of therapeutic success.[36–39] A serum IgG level greater than 1.5 times the upper normal limit is also one of the primary diagnostic criteria for autoimmune hepatitis.[35] The "chemical nose" system could be trained to distinguish between samples containing various levels and ratios of protein commonly found in the serum. The high turbidity of human serum interferes with spectrophotometric analysis of gold nanoparticles, and therefore samples were pre-diluted 1:20 in 1/4× PBS until a range of spectral responses could be distinguished. To obtain serum samples with elevated globulins, normal adult male serum was diluted in 1/4× PBS containing a pre-determined concentration of human IgG. The normal serum was then diluted in the same volume of 1/4× PBS without IgG to serve as a baseline comparison. The concentration of IgG in the diluent PBS was calculated to simulate the dilution of a high IgG serum sample in IgG-free PBS. The concentrations of IgG chosen for elevated and baseline samples were based on average IgG levels in healthy adult males[62] and represent an approximate two-fold increase. Diluted serum samples containing the elevated or baseline IgG levels were then mixed with the "chemical nose" solution. The resulting average absorption curves for 8 replicates are shown in Fig. 6A. The vertical shift in the curve position relative to the 1/4× PBS control indicates that the overall absorbance was significantly higher, likely due to the slight sample turbidity. However, when normalized against a baseline absorbance at 800 nm, a two-tailed t-test reveals that the peak height for serum samples containing elevated IgG was significantly lower compared to the baseline serum sample ($p < 0.01$). The PCA biplot in Fig. 6B demonstrates the separation of both groups based on the features of their absorbance spectra.

Conclusion

We demonstrated that the differential effects of various proteins on gold nanoparticle absorption spectra can be used to detect, identify, and quantify proteins in aqueous solutions, mixtures, and complex media such as human serum. We also noted the effect of ionic strength on this response and optimized the conditions for detection of nanomolar protein concentrations. Variations in the concentration-dependent response between proteins suggest several regimes which can stabilize or aggregate gold nanoparticles without surface functionalization. Two different nanoparticle morphologies with different aggregation behaviours were combined in one "chemical nose" solution for increased discriminatory potential, as previously demonstrated only in bacteria. Using PCA, several different proteins could be distinguished at nanomolar levels based on variations in the absorbance spectra of gold nanoparticles following ambient incubation. The binary mixtures of these proteins were also distinguishable and showed trends related to the mole fraction abundance of each protein. Finally, we demonstrated a novel method for protein analysis in complex media by successfully distinguishing serum samples with and without elevated IgG levels. This technique can be further improved by including more nanoparticle morphologies, thereby increasing the variety of observable

 This journal is © The Royal Society of Chemistry 2016

Published on 15 July 2016. Downloaded by Harvard University on 14/10/2016 16:45:31.

responses. Specifically, while some proteins do not induce noticeable aggregation with branched or spherical particles, varying other parameters such as particle size, charge, or surface coatings may increase the total number of detectable proteins. Future investigations will also seek to characterize these aggregation behaviours to enhance detection capabilities for various research, clinical, and consumer-level applications.

Methods

Materials

Gold(III) chloride hydrate ($HAuCl_4{\cdot}xH_2O$), cetyltrimethylammonium bromide (CTAB), sodium borohydride, silver nitrate, hydrochloric acid, nitric acid, sodium hydroxide, L-ascorbic acid, bovine serum albumin (A2153), albumin from human serum (A1653), IgG from human serum (I4506), fibrinogen from human plasma (F3879), lysozyme from chicken egg white (L6876), human hemoglobin (H7379) and human serum (H4522) were purchased from Sigma-Aldrich (Oakville, ON, Canada). Trisodium citrate dihydrate and BupH phosphate buffered saline packs were purchased from Thermo Fisher Scientific (Burlington, ON, Canada). Sterile UV-star 96-well microplates, scintillation vials (20 mL), sodium chloride (ACS grade), Nalgene sterilization filter units (0.2 μm pore size), 15 mL polypropylene centrifuge tubes, and 1.7 mL polypropylene microcentrifuge tubes were purchased from VWR (Mississauga, ON, Canada). 400 mesh formvar/carbon coated copper grids were purchased from Canemco Inc. (Gore, QC, Canada). All procured chemicals were used without further purification. The 20 mL vials used for gold nanoseed synthesis were cleaned using 12 M sodium hydroxide and larger glassware was cleaned using aqua regia as described in a previously published protocol.[63] Water used for the preparation of solutions was purified using a Millipore water filtration system to an electrical resistivity greater than 15 MΩ cm.

Synthesis of gold nanoparticles

CTAB-coated gold nanoparticles were synthesized according to a previously published protocol.[47] All synthesis solutions were prepared in Millipore water (>15 MΩ cm). Briefly, a gold seed precursor was prepared by adding 60 μL of ice-cold sodium borohydride to a solution containing 18.812 mL of Millipore water, 188 μL of 10 mg mL^{-1} gold(III) chloride, and 1 mL of 2 mM trisodium citrate under vigorous stirring. Following addition of sodium borohydride, the solution was stirred for 1 minute and left to mature overnight under dark ambient conditions. The nanoparticle growth solution was prepared under moderate stirring by adding 8.974 mL of 11 mM gold chloride, 1.344 mL of 5 mM silver nitrate, and 1.442 mL of 100 mM L-ascorbic acid to 210 mL of either 1.47 mM or 7.33 mM CTAB (for spherical and branched nanoparticles respectively). Finally, 5.6 mL or 2.24 mL of the gold seed precursor (for spherical and branched nanoparticles respectively) was added to the solution and stirred for an additional 1.5 minutes, at which point the solution was incubated overnight under dark ambient conditions. The final nanoparticle solution was pelleted *via* centrifugation and resuspended in 1 mM CTAB solution.

Protein solutions

Prior to reconstitution of lyophilized proteins, BSA, HSA, IgG, fibrinogen, lysozyme, and hemoglobin were stored at −5 °C or −20 °C, as per supplier's recommendation. Fresh protein solutions were prepared prior to each experiment. Solutions were prepared by weighing the appropriate amounts of protein into a microcentrifuge tube, and reconstituting in a calculated volume of purified water, sterile saline, or sterile PBS, to the desired final concentration. Lower ionic strength saline and PBS (1/4× and 1/16×) were prepared by diluting stock (1×) NaCl and PBS solutions (I = 450 mM) in Millipore H_2O at 1 : 3 or 1 : 15 ratios. After reconstitution, protein concentrations were adjusted by measuring absorbance at 280 nm (A_{280}) using an Epoch™ Microplate Spectrophotometer. Molar concentrations were determined using the Beer–Lambert Law:

$$A = \varepsilon \times l \times c$$

where A is the optical density of the sample, ε is the molar absorption coefficient of the protein obtained from the supplier or literature (Table S2†), l is the optical path length, and c is the molar concentration of the protein solution. Serial dilutions were performed to obtain solutions varying in the concentration from 450 μM to 27.5 nM. After adding 200 μL of the gold nanoparticle solution to 100 μL of each protein sample, the final protein concentrations were one third the normalized concentration, such that final solutions ranged from 150 μM to 9.2 nM. The final concentrations following dilution in the 96-well plate were confirmed by adding 200 μL of Millipore H_2O to 100 μL of the respective protein dilution, and measuring absorbance at 280 nm. Due to limitations in A_{280} quantification, protein concentrations were calculated directly from absorbances where the absorbance was in the linear range of the spectrophotometer (0.1–2.0), and extrapolated for samples beyond this range. Protein concentrations presented in the Results and discussion section represent molar concentrations following the 1/3 dilution, as determined using A_{280}. For protein identification assays, protein solutions were adjusted to a final concentration of 4.5 μM using A_{280} (Table S2†), and diluted 1/10 in 1/4× PBS for a final concentration of 450 nM. After adding 200 μL of the gold nanoparticle solution to 100 μL of each protein identification sample, the final protein concentration was 150 nM. For mixtures of HSA and IgG, individual protein concentrations were first adjusted to 450 nM as previously described, then mixed by volume to obtain the desired mole fractions of HSA and IgG such that the total protein concentration following addition of nanoparticles was 150 nM.

Serum preparation with IgG

Human serum samples for baseline IgG levels were diluted 20× in 1/4× PBS without any added protein. Serum samples for elevated IgG levels were diluted 20× in 1/4× PBS containing

Published on 15 July 2016. Downloaded by Harvard University on 14/10/2016 16:45:31.

3.42 μM IgG. The resultant IgG concentrations prior to incubation with gold nanoparticles were approximately 3.25 μM for the baseline serum (based on average IgG concentrations for human adult males) and 6.5 μM for high the IgG serum, a two-fold increase assuming a mean total IgG concentration of 65 μM in healthy adult males.[62]

Protein–gold incubation

The concentration-dependent response, protein identification, and serum experiments were assessed spectrophotometrically in a transparent 96-well plate. 100 μL of each protein sample or solvent control was added to the 96-well plate. Triplicate samples for each dilution were used for the concentration-dependent response, and eight replicates were used for identification and serum tests. 200 μL of the gold nanoparticle solution was then added to each well containing protein or control solution. Plates were then placed on a Stovall Belly Dancer orbital shaker (Peosta, IA, USA) for 2 minutes prior to 20 hour incubation in the dark at room temperature. Following incubation, an Epoch™ Microplate Spectrophotometer (Winooski, VT, USA) was used to obtain spectral scans for each well containing gold nanoparticles. Spectra were collected from 300–999 nm wavelengths, in increments of 1 nm.

Quantifying the gold nanoparticle response

The extent of gold nanoparticle aggregation was quantified by monitoring changes in peak absorbance relative to the solvent control. First, the position of the absorbance peak for the 1/4× PBS control (1° peak in wavelength nanometers) was determined from control spectral scans. Absorbance values at the 1° peak position were then noted for samples containing protein. The baseline absorbance at 800 nm was then determined for each sample. The peak height was calculated by subtracting each sample's baseline absorbance (800 nm) from the sample's absorbance at the 1° peak position:

$$\text{height}_{\text{sample}} = A_{\text{sample}}\ (1^\circ \text{ peak position}) - A_{\text{sample}}\ (800\ \text{nm})$$

The peak heights were then normalized against the control to obtain a normalized response for each protein sample:

$$\text{Normalized sample response} = \text{height}_{\text{control}} - \text{height}_{\text{sample}}$$

Statistical significance between peak heights for baseline and elevated IgG serum samples was determined using Microsoft Excel® *via* an independent two-tailed heteroscedastic *t*-test.

Protein classification

Principal Component Analysis (PCA) was conducted using MATLAB®. Protein solutions were grouped based on the resultant gold nanoparticle absorbance spectrum. Due to the broad extent of spectral shifts observed during protein-induced aggregation, all 700 wavelengths of the spectrum (300–999 nm) were used for classification. Raw absorbance spectra were used without manual pre-processing. Only built-in pre-processing was used within MATLAB® to center observations based on variable means. Confidence ellipses (95%) were also calculated using MATLAB®.

Transmission electron microscopy

Gold nanoparticle sizes and shapes were confirmed using a Phillips (Eindhoven, The Netherlands) CM10 TEM. Copper TEM grids (400 mesh formvar/carbon coated) were prepared under ambient conditions by overnight evaporation of a 5 μL droplet of the gold nanoparticle solution directly onto a grid. TEM micrographs were analyzed using ImageJ.

Author contributions

The manuscript was written through contributions of all authors. All authors have given approval to the final version of the manuscript.

Funding sources

This work was financially supported by the Natural Sciences and Engineering Research Council of Canada (NSERC). J. L. R. is grateful for the NSERC Canada Graduate Scholarship – Master's, and for the Waterloo Institute for Nanotechnology (WIN) Nanofellowship. M. S. V. is grateful for the NSERC Vanier Canada Graduate Scholarship and the Banting Postdoctoral Fellowship.

Conflict of interest

The authors declare no competing financial interests.

Abbreviations

BSA	Bovine serum albumin
HSA	Human serum albumin
IgG	Immunoglobulin G
Fib	Fibrinogen
Lyz	Lysozyme
Hgb	Hemoglobin
PCA	Principal component analysis
AGR	Albumin/globulin ratio
TEM	Transmission electron microscopy
PBS	Phosphate buffered saline
OD	Optical density

References

1 G. L. Hortin, S. A. Carr and N. L. Anderson, *Clin. Chem.*, 2010, **56**, 149–151.
2 N. L. Anderson, *Clin. Chem.*, 2010, **56**, 177–185.
3 J. F. Rusling, C. V. Kumar, J. S. Gutkind and V. Patel, *Analyst*, 2010, **135**, 2496–2511.

 This journal is © The Royal Society of Chemistry 2016

Published on 15 July 2016. Downloaded by Harvard University on 14/10/2016 16:45:31.

4 J. López-Barea and J. L. Gómez-Ariza, *Proteomics*, 2006, **6**(Suppl 1), S51–S62.
5 I. Palchetti and M. Mascini, *Analyst*, 2008, **133**, 846–854.
6 A. J. Van Hengel, *Anal. Bioanal. Chem.*, 2007, **389**, 111–118.
7 S. Rastogi, P. D. Dwivedi, S. K. Khanna and M. Das, *Food Control*, 2004, **15**, 287–290.
8 S. F. Kingsmore, *Nat. Rev. Drug Discovery*, 2006, **5**, 310–320.
9 M. S. Verma, J. L. Rogowski, L. Jones and F. X. Gu, *Biotechnol. Adv.*, 2015, **33**, 666–680.
10 J. Wang and X. Qu, *Nanoscale*, 2013, **5**, 3589–3600.
11 L. M. Bellan, D. Wu and R. S. Langer, *Wiley Interdiscip. Rev.: Nanomed. Nanobiotechnol.*, 2011, **3**, 229–246.
12 K. M. Mayer and J. H. Hafner, *Chem. Rev.*, 2011, **111**, 3828–3857.
13 S. Szunerits and R. Boukherroub, *Chem. Commun.*, 2012, **48**, 8999.
14 P. K. Jain, K. S. Lee, I. H. El-Sayed and M. A. El-Sayed, *J. Phys. Chem. B*, 2006, **110**, 7238–7248.
15 P. K. Jain and M. A. El-Sayed, *Chem. Phys. Lett.*, 2010, **487**, 153–164.
16 S. K. Ghosh and T. Pal, *Chem. Rev.*, 2007, **107**, 4797–4862.
17 D. F. Moyano, S. Rana, U. H. F. Bunz and V. M. Rotello, *Faraday Discuss.*, 2011, **152**, 33–42.
18 M. Cui, R. Liu, Z. Deng, G. Ge, Y. Liu and L. Xie, *Nano Res.*, 2013, **7**, 345–352.
19 R. Cukalevski, S. A. Ferreira, C. J. Dunning, T. Berggård and T. Cedervall, *Nano Res.*, 2015, **8**, 2733–2743.
20 S. R. Saptarshi, A. Duschl and A. L. Lopata, *J. Nanobiotechnol.*, 2013, **11**, 26.
21 S. H. Brewer, W. R. Glomm, M. C. Johnson, M. K. Knag and S. Franzen, *Langmuir*, 2005, **21**, 9303–9307.
22 S. Dominguez-Medina, S. McDonough, P. Swanglap, C. F. Landes and S. Link, *Langmuir*, 2012, **28**, 9131–9139.
23 J. Deka, A. Paul and A. Chattopadhyay, *J. Phys. Chem. C*, 2009, **113**, 6936–6947.
24 D. Zhang, O. Neumann, H. Wang, V. M. Yuwono, A. Barhoumi, M. Perham, J. D. Hartgerink, P. Wittung-Stafshede and N. J. Halas, *Nano Lett.*, 2009, **9**, 666–671.
25 M. Tirado-Miranda, A. Schmitt, J. Callejas-Fernández and A. Fernández-Barbero, *Eur. Biophys. J.*, 2003, **32**, 128–136.
26 X. Wang, Y. Xu, X. Xu, K. Hu, M. Xiang, L. Li, F. Liu and N. Li, *Talanta*, 2010, **82**, 693–697.
27 Y. T. Ho, B. Poinard, E. L. L. Yeo and J. C. Y. Kah, *Analyst*, 2015, **140**, 1026–1036.
28 C. M. Stoscheck, *Anal. Biochem.*, 1987, **160**, 301–305.
29 M. S. Verma, S. C. Wei, J. L. Rogowski, J. M. Tsuji, P. Z. Chen, C. W. Lin, L. Jones and F. X. Gu, *Biosens. Bioelectron.*, 2016, **83**, 115–125.
30 M. S. Verma, P. Z. Chen, L. Jones and F. X. Gu, *Sens. Bio-Sensing Res.*, 2015, **5**, 13–18.
31 M. S. Verma, P. Z. Chen, L. Jones and F. X. Gu, *Biosens. Bioelectron.*, 2014, **61**, 386–390.
32 K. Saha, S. S. Agasti, C. Kim, X. Li and V. M. Rotello, *Chem. Rev.*, 2012, **112**, 2739–2779.
33 R. L. Phillips, O. R. Miranda, C.-C. You, V. M. Rotello and U. H. F. Bunz, *Angew. Chem., Int. Ed.*, 2008, **47**, 2590–2594.
34 E. M. Hennes, M. Zeniya, A. J. Czaja, A. Parés, G. N. Dalekos, E. L. Krawitt, P. L. Bittencourt, G. Porta, K. M. Boberg, H. Hofer, F. B. Bianchi, M. Shibata, C. Schramm, B. Eisenmann de Torres, P. R. Galle, I. McFarlane, H. Dienes and A. W. Lohse, *Hepatology*, 2008, **48**, 169–176.
35 M. P. Manns, A. J. Czaja, J. D. Gorham, E. L. Krawitt, G. Mieli-Vergani, D. Vergani and J. M. Vierling, *Hepatology*, 2010, **51**, 2193–2213.
36 X.-J. Du, L.-L. Tang, Y.-P. Mao, Y. Sun, M.-S. Zeng, T.-B. Kang, W.-H. Jia, A.-H. Lin and J. Ma, *PLoS One*, 2014, **9**, e94473.
37 M. Shibutani, K. Maeda, H. Nagahara, H. Ohtani, Y. Iseki, T. Ikeya, K. Sugano and K. Hirakawa, *BMC Cancer*, 2015, **15**, 347.
38 B. N. Azab, V. R. Bhatt, S. Vonfrolio, R. Bachir, V. Rubinshteyn, H. Alkaied, A. Habeshy, J. Patel, A. I. Picon and S. W. Bloom, *Am. J. Surg.*, 2013, **206**, 764–770.
39 B. Suh, S. Park, D. W. Shin, J. M. Yun, B. Keam, H.-K. Yang, E. Ahn, H. Lee, J. H. Park and B. Cho, *Ann. Oncol.*, 2014, **25**, 2260–2266.
40 R. Pamies, J. G. H. Cifre, V. F. Espín, M. Collado-González, F. G. D. Baños and J. G. De La Torre, *J. Nanopart. Res.*, 2014, **16**, 2376.
41 C. Pfeiffer, C. Rehbock, D. Hühn, C. Carrillo-Carrion, D. J. de Aberasturi, V. Merk, S. Barcikowski and W. J. Parak, *J. R. Soc., Interface*, 2014, **11**, 20130931.
42 S. P. Boulos, T. A. Davis, J. A. Yang, S. E. Lohse, A. M. Alkilany, L. A. Holland and C. J. Murphy, *Langmuir*, 2013, **29**, 14984–14996.
43 X. Zhang, M. R. Servos and J. Liu, *J. Am. Chem. Soc.*, 2012, **134**, 9910–9913.
44 A. R. Ferhan, L. Guo and D.-H. Kim, *Langmuir*, 2010, **26**, 12433–12442.
45 M. Boulet, M. Britten and F. Lamarche, *Food Hydrocoll.*, 2000, **14**, 135–144.
46 S. Pasche, J. Vörös, H. J. Griesser, N. D. Spencer and M. Textor, *J. Phys. Chem. B*, 2005, **109**, 17545–17552.
47 M. S. Verma, P. Z. Chen, L. Jones and F. X. Gu, *RSC Adv.*, 2014, **4**, 10660–10668.
48 M. S. Verma, J. M. Tsuji, B. Hall, P. Z. Chen, J. Forrest, L. Jones and F. X. Gu, *Sens. Bio-Sensing Res.*, 2016, **10**, 15–19.
49 S. H. De Paoli Lacerda, J. J. Park, C. Meuse, D. Pristinski, M. L. Becker, A. Karim and J. F. Douglas, *ACS Nano*, 2010, **4**, 365–379.
50 A. Chaudhary, A. Gupta, S. Khan and C. K. Nandi, *Phys. Chem. Chem. Phys.*, 2014, **16**, 20471–20482.
51 Z. J. Deng, M. Liang, I. Toth, M. J. Monteiro and R. F. Minchin, *ACS Nano*, 2012, **6**, 8962–8969.
52 J. U. Lee, A. H. Nguyen and S. J. Sim, *Biosens. Bioelectron.*, 2015, **74**, 341–346.
53 J. A. Jamison, E. L. Bryant, S. B. Kadali, M. S. Wong, V. L. Colvin, K. S. Matthews and M. K. Calabretta, *J. Nanopart. Res.*, 2011, **13**, 625–636.
54 M. A. Dobrovolskaia, A. K. Patri, J. Zheng, J. D. Clogston, N. Ayub, P. Aggarwal, B. W. Neun, J. B. Hall and

S. E. McNeil, *Nanomed. Nanotech., Biol. Med.*, 2009, **5**, 106–117.
55 E. Casals, T. Pfaller, A. Duschl, G. J. Oostingh and V. Puntes, *ACS Nano*, 2010, **4**, 3623–3632.
56 C. D. Walkey, J. B. Olsen, H. Guo, A. Emili and W. C. W. Chan, *J. Am. Chem. Soc.*, 2012, **134**, 2139–2147.
57 H. Pan, M. Qin, W. Meng, Y. Cao and W. Wang, *Langmuir*, 2012, **28**, 12779–12787.
58 X. Jiang, J. Jiang, Y. Jin, E. Wang and S. Dong, *Biomacromolecules*, 2005, **6**, 46–53.
59 J. E. Gagner, M. D. Lopez, J. S. Dordick and R. W. Siegel, *Biomaterials*, 2011, **32**, 7241–7252.
60 N. Thioune, N. Lidgi-Guigui, M. Cottat, A.-M. Gabudean, M. Focsan, H.-M. Benoist, S. Astilean and M. L. Chapelle, *Gold Bull.*, 2013, **46**, 275–281.
61 K. Siriwardana, A. Wang, K. Vangala, N. Fitzkee and D. Zhang, *Langmuir*, 2013, **29**, 10990–10996.
62 J. Stoop, B. J. Zegers, P. C. Sander and R. E. Ballieux, *Clin. Exp. Immunol.*, 1969, **4**, 101–112.
63 J. Liu and Y. Lu, *Nat. Protoc.*, 2006, **1**, 246–252.

Published on 15 July 2016. Downloaded by Harvard University on 14/10/2016 16:45:31.

This journal is © The Royal Society of Chemistry 2016